Growth of the Afanasy Nikitin seamount and its relationship with the 85°E Ridge, northeastern Indian Ocean

K S Krishna[1,*], J M Bull[2], O Ishizuka[3], R A Scrutton[4], S Jaishankar[1] and V K Banakar[1]

[1]*CSIR – National Institute of Oceanography, Dona Paula, Goa 403 004, India.*
[2]*School of Ocean and Earth Science, University of Southampton, National Oceanography Centre Southampton, Southampton SO14 3ZH, UK.*
[3]*Geological Survey of Japan/AIST, Ibaraki, 305-8567, Japan.*
[4]*School of Geosciences, Edinburgh University, Edinburgh, EH9 3JW, UK.*
[*]*Corresponding author. e-mail: krishna@nio.org*

The Afanasy Nikitin seamount (ANS) is a major structural feature (400 km-long and 150 km-wide) in the Central Indian Basin, situated at the southern end of the so-called 85°E Ridge. Combined analyses of new multibeam bathymetric, seismic reflection and geochronological data together with previously described magnetic data provide new insights into the growth of the ANS through time, and its relationship with the 85°E Ridge. The ANS comprises a main plateau, rising 1200 m above the surrounding ocean floor (4800 m), and secondary elevated seamount highs, two of which (lie at 1600 and 2050 m water depths) have the morphology of a guyot, suggesting that they were formed above or close to sea-level. An unbroken sequence of spreading anomalies 34 through 32n.1 identified over the ANS reveal that the main plateau of the ANS was formed at 80–73 Ma, at around the same time as that of the underlying oceanic crust. The $^{40}Ar/^{39}Ar$ dates for two basalt samples dredged from the seamount highs are consistent, within error, at 67 Ma. These results, together with published results of late Cretaceous to early Cenozoic Indian Ocean plate reconstructions, indicate that the Conrad Rise hotspot emplaced both the main plateau of the ANS and Conrad Rise (including the Marion Dufresne, Ob and Lena seamounts) at 80–73 Ma, close to the India–Antarctica Ridge system. Subsequently, the seamount highs were formed by late-stage volcanism c. 6–13 Myr after the main constructional phase of the seamount plateau. Flexural analysis indicates that the main plateau and seamount highs of the ANS are consistent with Airy-type isostatic compensation, which suggest emplacement of the entire seamount in a near spreading-center setting. This is contrary to the flexural compensation of the 85°E Ridge further north, which is interpreted as being emplaced in an intraplate setting, i.e., 25–35 Myr later than the underlying oceanic crust. Therefore, we suggest that the ANS and the 85°E Ridge appear to be unrelated as they were formed by different mantle sources, and that the proximity of the southern end of the 85°E Ridge to the ANS is coincidental.

Keywords. Afanasy Nikitin seamount; 85°E Ridge; Indian Ocean; $^{40}Ar/^{39}Ar$ dating; Conrad Rise hotspot; Marion Dufresne seamount.

J. Earth Syst. Sci. **123**, No. 1, February 2014, pp. 33–47

1. Introduction

Within the northern Indian Ocean the Chagos-Laccadive, 85°E and 90°E ridges are striking examples of aseismic ridges. These linear or curvi-linear features represent excess volcanism over lengths of thousands of kilometres, emplaced over periods of tens of millions of years. The Afanasy Nikitin seamount (ANS), a major seamount in the central Indian Basin (figure 1), has been interpreted as a product of excessive late Cretaceous volcanism at or near the India–Antarctica (spreading) Ridge, and is usually considered as the southernmost part of the 85°E Ridge hotspot track (Curray and Munasinghe 1991; Müller *et al.* 1993; Krishna 2003). Although the 85°E Ridge runs parallel to the 90°E Ridge, its precise track is curious because its morphology changes and, in places, its surface expression is indistinct, but also because it shows a curvature of about 250 km seaward of southeast Sri Lanka, which is not apparent in either the track to the east, the 90°E Ridge, or the one to the west, the Chagos-Laccadive Ridge. Other alternatives suggested for the origin of the 85°E Ridge, include fossil ridge, scars left by plate reorganisations, continental sliver, etc., but these are not compatible with the recently inferred spreading fabric of the oceanic lithosphere in the Bay of Bengal determined from magnetic anomaly distribution, satellite gravity data and seismic structure (Krishna *et al.* 2009a; Radhakrishna *et al.* 2012).

Curray and Munasinghe (1991) assigned the 85°E Ridge track including the ANS to the Crozet hotspot, but Mahoney *et al.* (1996) identified that the geochemistry of lavas sampled from the ANS does not obviously support the Crozet plume model. Subsequently, Müller *et al.* (1993) attributed the track to a hotspot lying presently at the Conrad Rise (Marion Dufresne, Lena and Ob seamounts), and this was later reaffirmed using a model based on a moving hotspot framework (O'Neill *et al.* 2003). In these models, the hotspot track (85°E Ridge and ANS) occurs as a continuous feature dating from about 100 to about 70 Ma, whereupon a northward jump of the spreading centre of the India–Antarctica Ridge is invoked at a time between anomalies 31 and 25 in order to isolate the hotspot on the Antarctic plate. However, there is no evidence found in the linear magnetic anomaly pattern for such a ridge jump at this time, rather observed a continuous north–south spreading process until the well-documented major reorganisation of spreading at 42 Ma and the creation of the southeast Indian Ridge (Liu *et al* 1983; Royer and Sandwell 1989; Royer et al. 1991; Krishna *et al* 1995, 2012). In summary, these models predict an age for the ANS of c. 75 Ma as an end-product of the 85°E Ridge, but there is no evidence of a ridge jump.

Previous work using rock samples and geophysical data has suggested that the ANS was formed in two phases, one close to the age of the underlying oceanic crust, the other phase being poorly constrained, but much later. Analyses of gravity and bathymetry data of the ANS (Karner and Weissel 1990; Paul *et al.* 1990) determined a low (2–5 km) elastic plate thickness (T_e) below the ANS and was interpreted as indicating that the seamount was emplaced close to the spreading center. Subsequently, Sborshchikov *et al.* (1995) studied the petrochemical data of the ANS and found that the main plateau of the seamount, comprised of basalts and picrite-basalts, formed on young oceanic crust during the late Cretaceous. Later more differentiated alkaline trachybasaltic to trachytic series of lava flows formed the cone-shaped volcanic edifices (seamount highs in figure 2) over the main plateau. The authors conjectured that volcanic activity either continued up to Palaeocene, or occurred in two stages, late Cretaceous and Paleocene. The Palaeocene age of the ANS was deduced (Sborshchikov *et al.* 1995) from the recovery of a nannofossil assemblage from chalk cement in conglomerates on seamount high 'A' (figure 2). This led Krishna (2003) to present a comprehensive tectonic model for the history of renewed magmatism at the ANS at ∼55 Ma and connection to the 85°E Ridge. This model envisages a short-lived magmatic event creating the main part of the ANS at the India–Antarctica Ridge during 80–73 Ma, with the Palaeocene component of the ANS as the southernmost expression of a younger 85°E Ridge, which originated from an unknown hotspot source. He further suggesting that the 85°E Ridge hotspot was active from about 85 Ma to about 55 Ma. Central to this argument is a Palaeocene age for part of the ANS and the Indian plate motion from late Cretaceous to early Tertiary.

In this paper we describe new $^{40}Ar/^{39}Ar$ dating results from dredged basalt samples which show that the late-stage volcanism of the ANS occurred at 67 Ma, which is at variance with the model of Krishna (2003) for the genesis of the ANS. In order to resolve this problem we investigate the emplacement process of the ANS through time and its relationship to the 85°E Ridge track using existing magnetic data and new multibeam

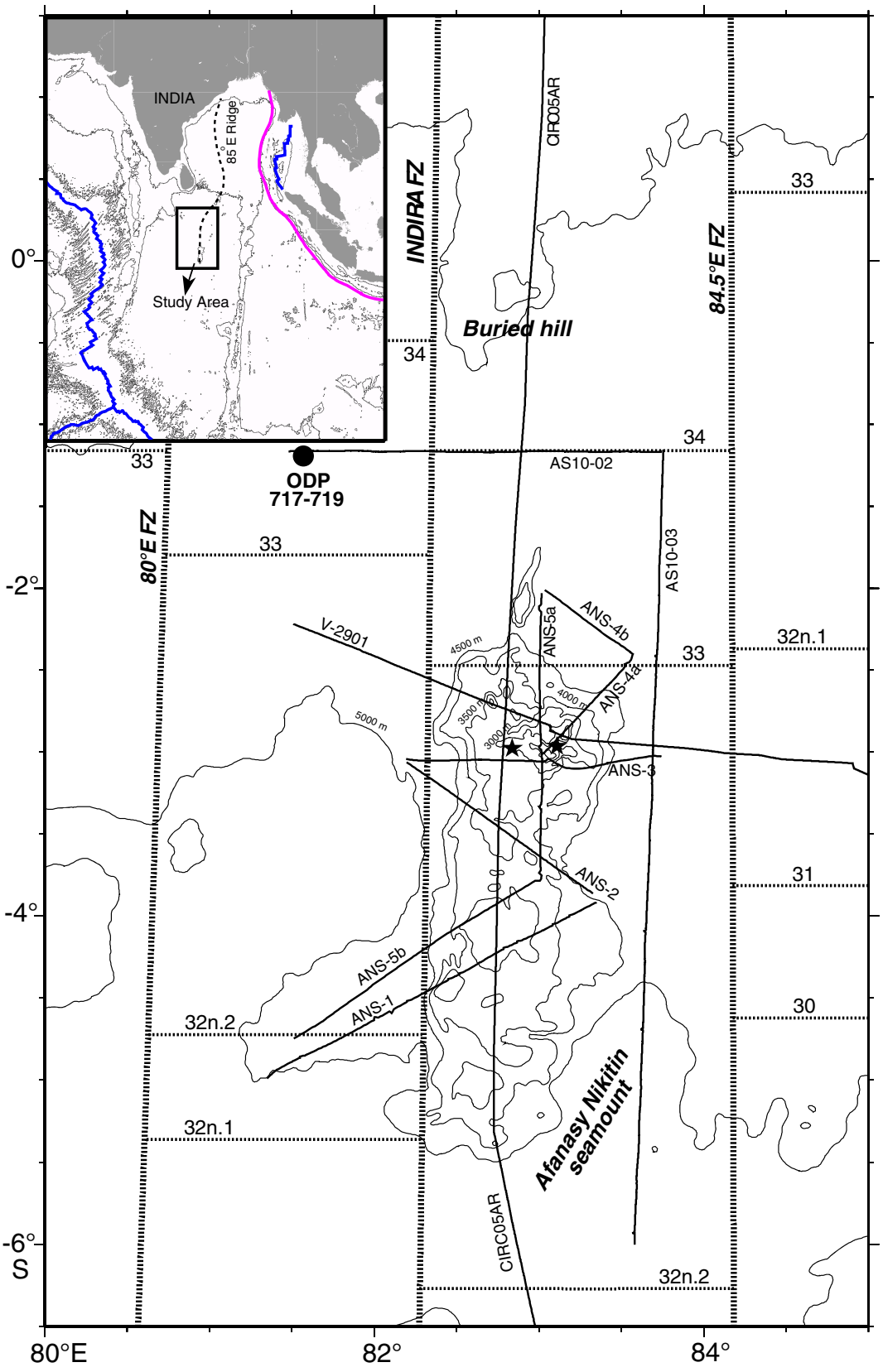

Figure 1. Location of the Afanasy Nikitin seamount (ANS) in the central Indian Basin. Bathymetric data (contour interval 500 m) from ETOPO5 show the general relief of the ANS and its adjacent ocean floor. Solid lines show the geophysical (seismic reflection, gravity and magnetic) profiles. Magnetic lineations A34 through A30 and fracture zones shown in the vicinity of the ANS are adopted after Bull (1990) and Krishna and Gopala Rao (2000). Stars show the location of dredge samples used for dating. Inset map shows the area of the present study in the northern Indian Ocean.

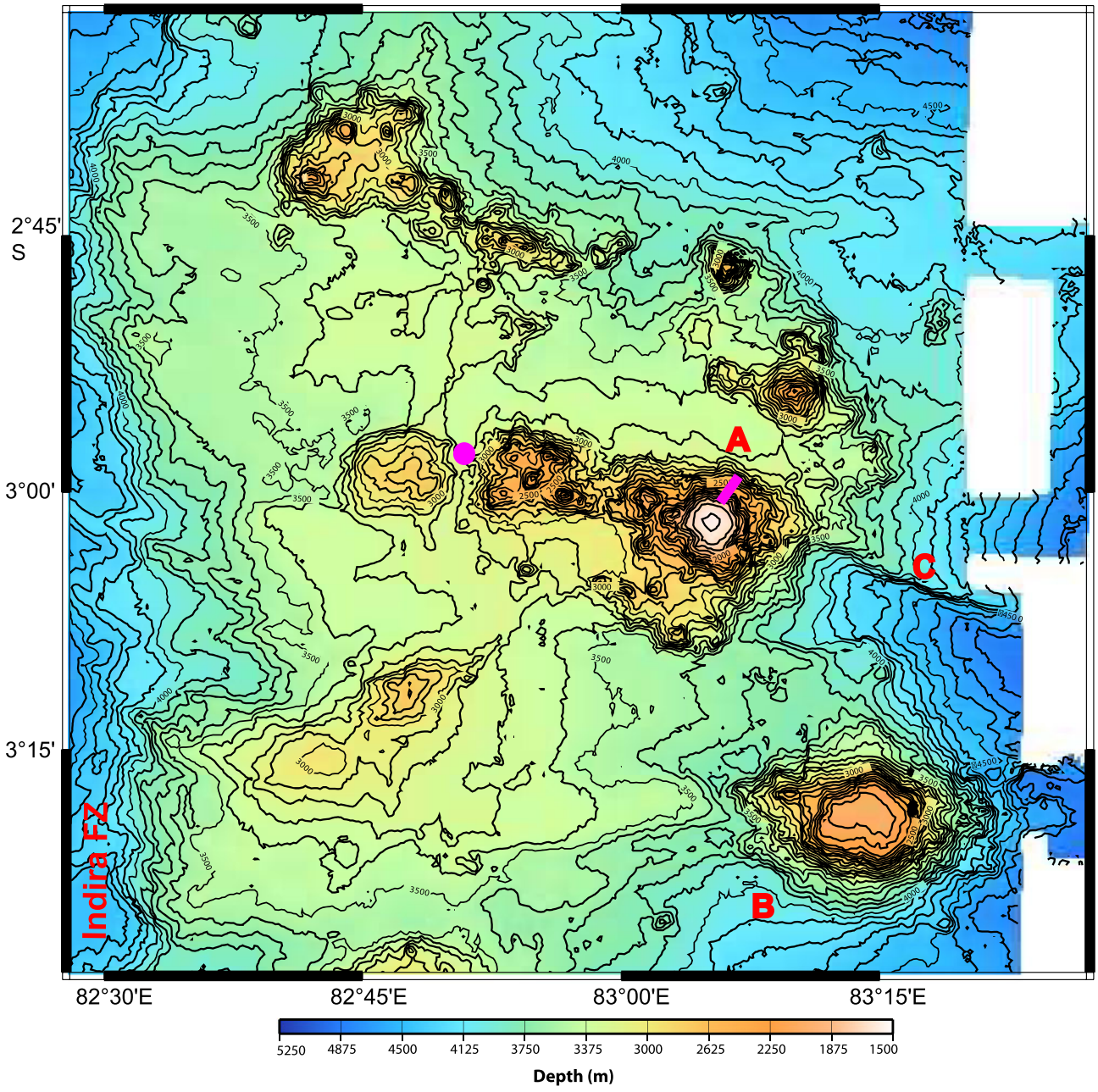

Figure 2. Multibeam data (contour interval 100 m) of the northern part of the ANS. Colour gradients assigned for the water depths are shown in the bottom of the figure. Notable flat-topped seamount highs are indicated (A and B), as is a fault (C). Solid (violet colour) circle indicates position of sample (CC2/ADR24) dredged, solid (violet colour) line the position of dredge that resulted in sample AFNCD28.

bathymetric, seismic reflection, geochemical and geochronological data.

2. Analysis of new multibeam bathymetric data

Multibeam bathymetric data collected over the northern part of the ANS (figure 2), reveal that seafloor topography of this part of the seamount varies from 1600 to 4800 m water depth and exhibits two scales of structures. Overall, the seamount rises to a 'main plateau' at about 3600 m water depth above the surrounding water depths of ∼4800 m (figure 2). This plateau forms the bulk of the ANS, extending from 2°15' to 5°30'S (figures 1 and 3). The plateau steps down rapidly on its western side by more than 1000 m in less than 15 km distance and terminates against the N–S oriented Indira Fracture Zone (figures 2, 4 and 5), whereas on the eastern side the plateau falls with a gentle gradient, and merges with the Miocene-age deformation related long-wavelength rises and depressions (Krishna *et al.* 1998, 2001).

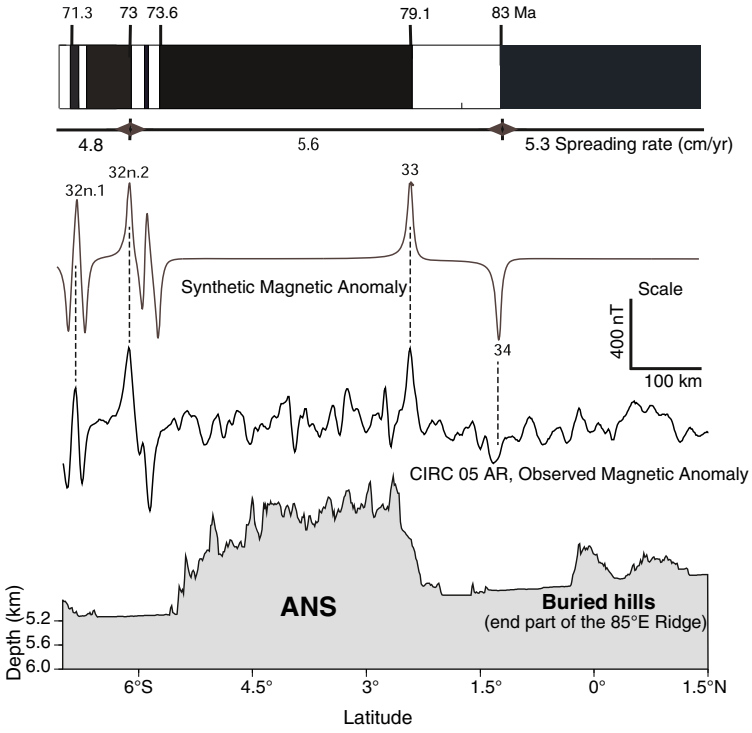

Figure 3. Seafloor topography and magnetic anomaly data along the profile CIRC 05AR running on top of the ANS. The anomalies are correlated with the synthetic magnetic anomaly profile for identification of spreading-type anomalies.

Superimposed on the main plateau are a number of elevated and faulted features (A–C in figure 2). Several of these secondary rises are aligned approximately N100°E, which is the orientation of the original spreading-centre fabric away from the seamount (Bull and Scrutton 1992), suggesting volcanism utilised these pre-existing weaknesses. One notable fault (C, in figure 2) has a slightly different orientation, trending in N120°E with a throw of up to 100 m. Two larger conical structures (seamount highs 'A' and 'B' in figure 2) are considered as major individual seamounts, and are now discussed further.

Seamount highs 'A' and 'B' rise to water depths of 1600 and 2050 m, respectively and their top surfaces are nearly flat and having the morphology of guyot (figure 2), suggesting that during their subsidence history these seamounts were close to sea-level and were affected by wave action (Banakar *et al.* 1997). Indeed, the summit (seamount high 'A') has sediment build-up of about 250 m (figures 4 and 5). Conglomerates containing freshwater phreatic cement embedding Terebratulinae casts and rounded basalt clasts, were found on the summit edge of this seamount and are thought to testify its exposure to sub-aerial high energy environment when it was emplaced (Sborshchikov *et al.* 1995; Banakar *et al.* 1997). There is evidence from nannofossil assemblages found within their calcareous cement, that the conglomerates are as young as Palaeocene in age (Sborshchikov *et al.* 1995). We have also found Palaeocene fossils (microplankton) in chalk from vugs in basalts dredged from the slopes of seamount 'A'. Overall, there are convincing evidences to show that the summit of seamount 'A' was at or near sea-level as recently as Palaeocene time, either as an eroded rock surface or as a calcareous sediment build-up. However, it is not possible to further constrain when within the Palaeocene the seamount was this shallow, and this also gives a minimum age for the seamount. The age of the seamount is addressed further from magnetic data in section 3 and from direct dating of basalt samples in section 5.

3. Spreading-type magnetic anomalies over the seamount

Magnetic anomaly profile, CIRC 05AR, orientated N–S over the top of the ANS (figure 1) is compared with a synthetic magnetic anomaly profile (figure 3) for the purpose of identifying seafloor spreading type anomalies, and thereby to assign an age to the ANS. The synthetic magnetic profile was prepared using 500 m thick normal and reverse polarity blocks, magnetisation strength of 0.01 A/m, paleolatitude of 40°S and half spreading rates ranging between 4.8 and 5.6 cm/yr (figure 3). Spreading anomalies 32n.1 and 32n.2 on south of the ANS and the anomalies 33 and 34 on north of the ANS are clearly observed (figure 3). Small-scale

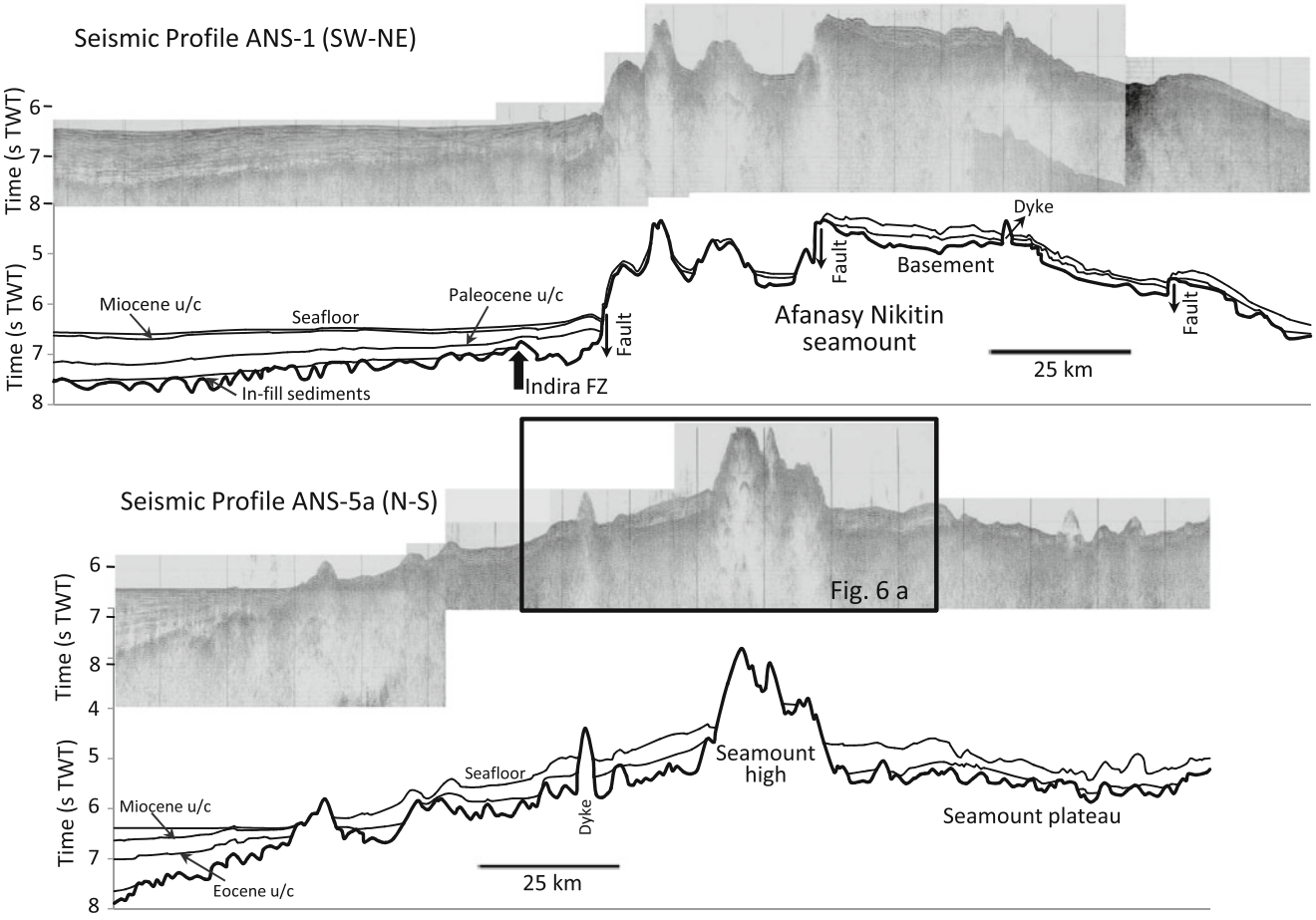

Figure 4. Seismic reflection profiles (ANS-1 and ANS-5a) and their interpretations show the internal structure of the ANS and its adjacent western region. Enlarged seismic section of the panel marked on profile ANS-5a is shown in figure 6(a).

tiny magnetic anomalies are also present, probably caused by the undulating basement morphology. The ANS main plateau is sitting on a long normally magnetized crustal block between anomalies 32n.2 and 33 (figure 3). Following the magnetic time scale of Cande and Kent (1995), it is found that the ANS is emplaced on an oceanic crust generated between 80 Ma in the north ANS and 73 Ma in the south (for more details, see Krishna and Gopala Rao 2000; Krishna 2003). An unbroken sequence of identified spreading anomalies 34 through 32.n.1 on CIRC 05AR suggests that the ANS was formed at 80–73 Ma concurrently with the generation of underlying oceanic crust.

4. Seismic structure of the seamount

Seismic reflection data acquired along profiles ANS-1, -2, -3, -4a, -4b and -5a over the ANS (figure 1) were investigated with a purpose of understanding the relevance of the basement morphology and sedimentation patterns to the growth of the seamount. Basement structure has been mapped (figures 4–7) and confirms the north–south extent of the main plateau for a distance of about 350 km between 2°15' and 5°30'S latitudes, with a width of approximately 140 km. On its western side the plateau is flanked by the Indira Fracture Zone along 82°10'E longitude, most clearly seen on profiles ANS-1 and -2 (figure 5). Between 3° and 4°S the plateau displays a number of north–south trending structures with geometry reminiscent of eastwards tilted blocks faulting down to the west (figure 5c). These structures cannot be traced northwards, where the faulted basement topography appears to be replaced or overprinted by a number of volcanic highs, including the individual, larger seamount highs 'A' and 'B' and prominent NNW–SSE and nearly E–W trending ridge features. The multibeam bathymetric data and seismic data show these features much more clearly (figures 2 and 6). Seismic profiles ANS-5a and -3 (figure 6) reveal the details of how the seamount high 'A' was emplaced onto the existing main plateau of the ANS. On the foot of the seamount high and towards the plateau about 0.6 s (TWT) thick sediments are present, while on top

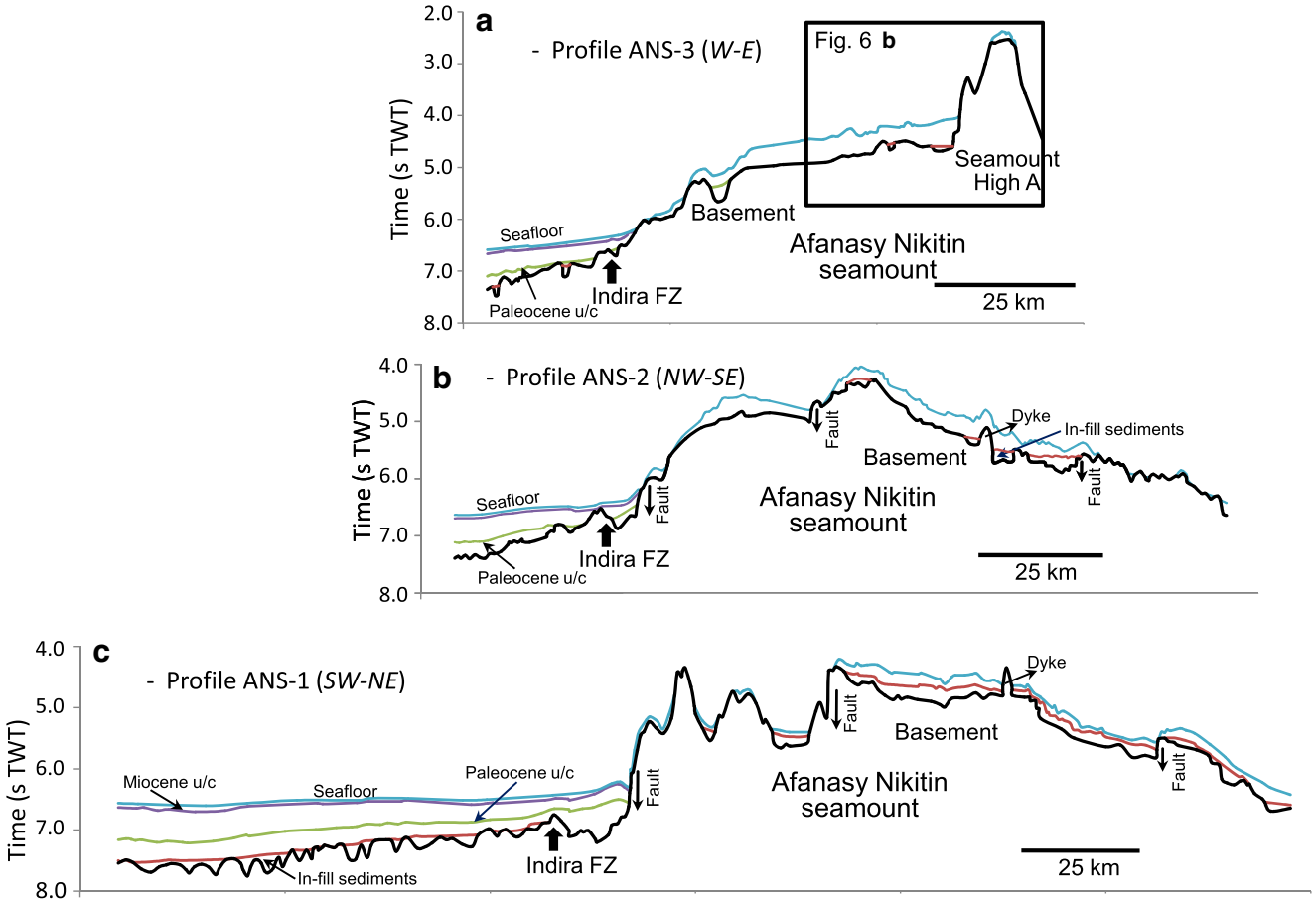

Figure 5. Line drawings of three seismic profiles (position illustrated in figure 1) crossing the Afanasy Nikitin seamount. The position of the Indira Fracture Zone (also termed as 82°E FZ) is indicated on the western margin of the seamount on each profile. Regional unconformities of Miocene and Palaeocene age overlap onto the flanks of the seamount. Seismic section of the panel marked on an interpreted profile ANS-3 is shown in figure 6(b).

and on the flanks of the seamount high almost no sediments are observed. Hence the flank locations were chosen for dredging of the rocks for geochemical and geochronological studies. In spite of variable morphological trends expression of the ANS, we observed the presence of a number of thrust faults (figures 5 and 6). These faults developed due to the ongoing (from 15.4 Ma to present) compressive deformation in the equatorial Indian Ocean (Krishna *et al.* 2009b). Exceptionally, a dyke-like feature seen on profile ANS-1 (figure 4) can be traced northwards through the area of volcanic highs and is seen again on profile ANS-5a (figure 5b and c). We have no seismic reflection profiles to the south of ANS-1, but bathymetric data in which slopes are steep to the west and gentler to the east suggesting that the dyke between 3° and 4°S extends to the south. There is also some suggestion in bathymetric data that the main plateau rises slightly towards the south, perhaps reflecting the trend of Neogene–Quaternary plate buckling as seen along profile AS10-03 (figure 7) (see Krishna *et al.* 1998, 2001).

The profiles ANS-1 and -5a also show how the basement rises gradually onto the main plateau from about 7.0 s TWT in the adjacent basin (figure 4). Sediments in the deep basin thin towards the seamount, and progressively onlap the gently rising basement. The stratigraphic pattern and basement geometry give no evidence for flexure of the oceanic basement towards the seamount that would be associated with substantial construction of the ANS in an intraplate setting, although small volcanic additions in an intraplate setting cannot be ruled out.

Sediment cover over the main plateau is remarkably regular, at about 0.6 s TWT (figures 4–7). Steep slopes, however, are commonly devoid of significant sediment cover, whilst the deep ocean basin typically contains thicknesses of 1.5 s TWT, reaching up to 2.0 s TWT to the east of the ANS. The seismic characteristics of the sediments lying on the seamount and in the adjacent basin are different, suggesting different depositional environments. The sediments on the main plateau are broadly divided into two sections: in the lower

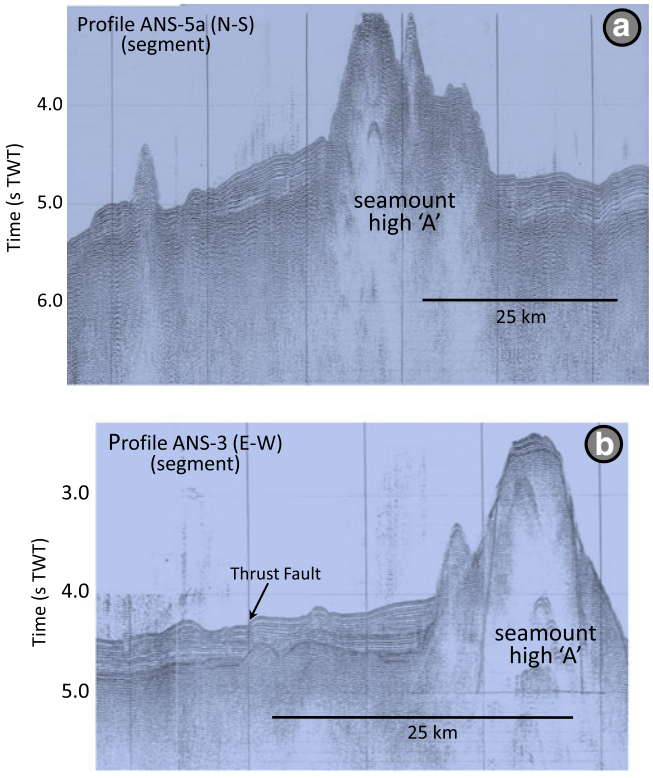

Figure 6. Enlarged seismic sections of the seamount 'A' imaged on profiles ANS-5a and -3. For specific locations, see figures 4 and 5.

section the reflectors are only weakly-continuous and sometimes disturbed, whereas in the upper section reflectors are more continuous and parallel. We interpret the plateau cover as a drape of pelagic sediments with a lofted turbidite component in its upper part (Redbourn *et al.* 1993). The sediments in the adjacent basin are broadly divided into three sections: a lower section infilling basement topography of strong, laterally continuous reflectors, a middle section of less strong and weakly-continuous reflectors, and an upper section of moderately strong and laterally-continuous reflectors. We identify these three sections with a lowermost pelagic infill, and then a mix of pelagic sediment and terrigeneous material derived from Indian landmass before the India–Asia collision, and finally distal deposits of the Bengal Fan as it encroached southwards. Following the seismic reflection character of the sedimentary section in the Bay of Bengal, Curray *et al.* (1982), Gopala Rao *et al.* (1997) and Michael and Krishna (2011) have interpreted the boundary below the post-collision sediments as a Palaeocene unconformity. This is the boundary where we would expect to see a stratigraphic relationship consistent with flexure if there was significant growth of the ANS in the Palaeocene, but we do not observe this (figures 4 and 5). Within the Bengal Fan sediment section we have mapped the deformation-related Miocene unconformity using stratigraphic onlaps (figures 4 and 5).

5. Analysis and dating of seamount basalt samples

Two basalt samples dredged from the flanks of the northern seamount complex 'A' (figure 2) were selected for dating by $^{40}Ar/^{39}Ar$ method. The first sample (CC2/ADR24) was dredged onboard *RV AA Sidorenko* (AAS) during cruise 59 from water depths between 3490 and 3200 m. The second sample (figure 8; AFNCD28) was from *RV Charles Darwin* (CD) cruise 28, collected along a dredge line (2°58'S, 83°6.5'E–3°01'S, 83°05'E) running up the north–east flank of the seamount high 'A' in water depths ranging from 2500 to 2000 m.

5.1 *Petrography*

AFNCD28 is a moderately-vesiculated (15–20%) plagioclase-phyric, clinopyroxene-olivine basalt with phenocrysts of plagioclase (7–9%, <8 mm), olivine (4–5%, 0.2–1 mm) and clinopyroxene (1–2%, <1 mm). Groundmass is mainly composed of plagioclase lath with swallowtail texture, olivine, and pyroxene with variolitic texture. While olivine phenocrysts were iddingsitized, plagioclase and clinopyroxene are mostly fresh.

The sample CC2/ADR24 has much fewer phenocrysts. This sample is moderately-vesiculated (15–20%) and sparsely-phyric olivine basalt with phenocrysts of olivine (4–5%, <0.5 mm) and plagioclase (<3%, <1.5 mm). Groundmass is dominated by plagioclase lath and pyroxene with variolitic texture. Even though some vesicles are filled with carbonate and iddingsitized olivine phenocrysts, the plagioclase and pyroxene in groundmass are fresh. Borisova *et al.* (2001) also studied basalts from the ANS, and found similar plagioclase-phyric and olivine-phyric basalts, with the plagioclase-phyric basalts being found at shallower depths, consistent with the new samples described here.

5.2 *Geochemistry*

Geochemical characteristics of samples recovered by the CD 28 cruise (sample AFNCD28) have been reported by Mahoney *et al.* (1996). The sample from the AAS-59 cruise (CC2/ADR24) shows similar characteristics as that of the AFNCD28 sample, i.e., OIB-like trace element signature enriched in highly incompatible element with

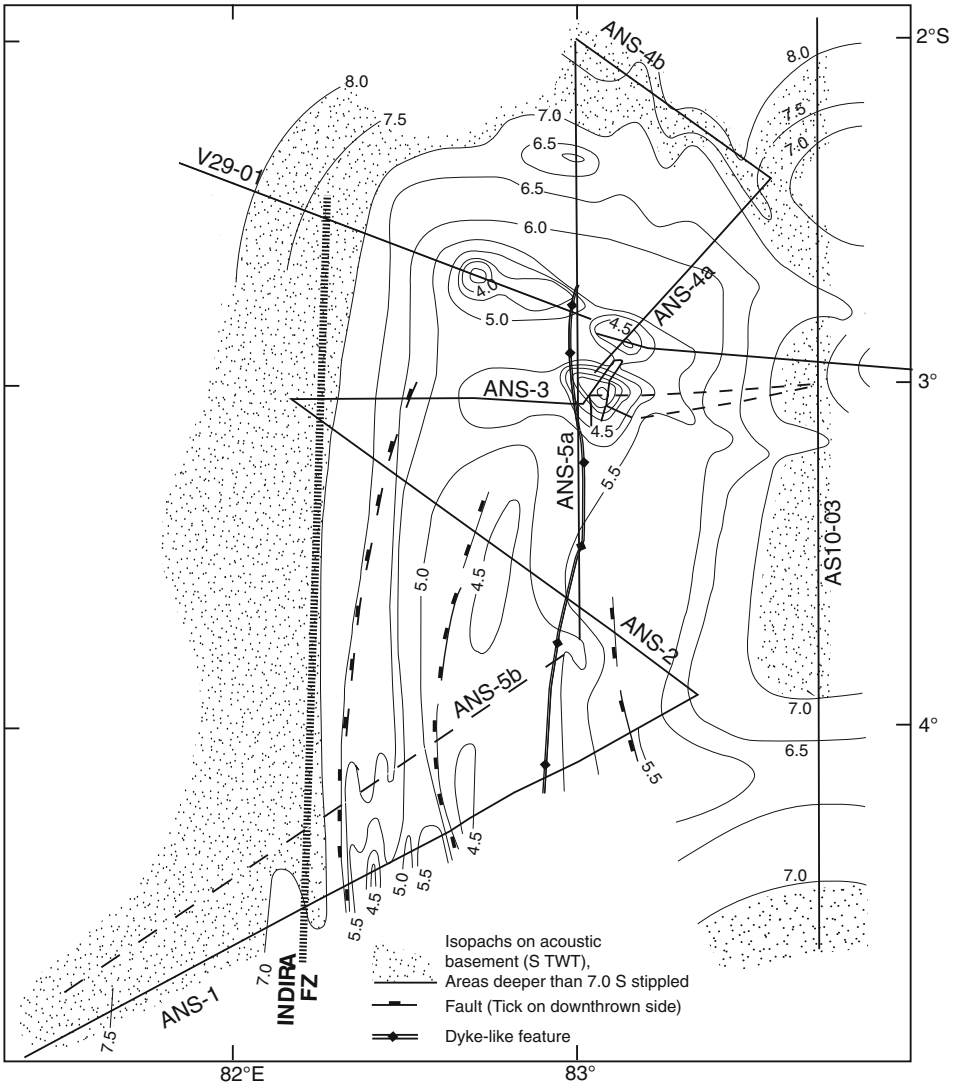

Figure 7. Depth to the basement contour map (seconds in TWT) of the ANS and adjacent areas. Solid lines show the seismic profiles used for the preparation of this contour map. Along the dashed line only gravity and magnetic data were acquired. In the northern part of the ANS, multibeam bathymetric data were used for mapping structural trends.

slightly higher Ba/Nb (21.7), La/Nb (0.98) and Ba/Th (153) relative to modern OIB. Isotopic characteristics of CC2/ADR24 show very low $^{206}Pb/^{204}Pb_{initial}$ of 17.23 and high $^{87}Sr/^{86}Sr_{initial}$ of 0.70672, i.e., extreme EM1 character similar to sample AFNCD28 (Mahoney *et al.* 1996). For sample CC2/ADR24, we assumed 67 Ma to calculate the initial ratios, whereas Mahoney *et al.* (1996) assumed 80 Ma – this difference in age results in only a small change in the isotopic ratios.

5.3 $^{40}Ar/^{39}Ar$ dating

Age determinations of volcanic rocks were carried-out using the $^{40}Ar/^{39}Ar$ geochronology facility at the Geological Survey of Japan/AIST following the analytical procedure described in Ishizuka *et al.* (2009). Methods and results of Ar isotopic analyses are presented in the Appendix. All errors for $^{40}Ar/^{39}Ar$ results are reported as 1-σ standard deviation.

Groundmass separate from sample CC2/ADR24 comprised 63.8% of total released gas and returned a plateau age of 67.36 ± 0.10 Ma (figure 9; table 1). Since consistently low atmospheric contamination for the steps defining a plateau produced a poorly-constrained isochron, a weighted average age of these steps is adopted as a reliable eruption age. Plagioclase separate from another sample AFNCD28 comprising middle to high temperature steps released 72.9% of total gas, and gave a well-defined age of 67.65 ± 0.08 Ma (figure 9; table 1). These two samples ages are indistinguishable within 2σ error.

Figure 8. Photograph of dredge samples collected on the north–east side of seamount high 'A' along a track 2°58'S, 83°6.5'E to 3°01'S, 83°05'E (dredge track is shown in figure 2). The large rock sample on the left of the image was analyzed (AFNCD28) and dated.

6. Discussion

6.1 *Growth of the ANS through time*

We have examined the water depths and geomorphology of the flat-topped 'guyot' type seamount highs 'A' and 'B' and other lower relief highs in the context of the subsidence history of the ANS as a whole (figure 2). If these seamount highs evolved along with the main plateau during 80–73 Ma (determined in correlations with the geomagnetic reversals model profile, figure 3) and subsided normally, the highs presently at <3000 m water depth would have formed above or close to the sea surface and subjected to the erosion processes by means of wave action and winds. However, only two seamount highs 'A' and 'B' lying currently at <2000 m water depth became guyots with the formation of flat-topped surfaces with associated slope gully patterns down to 2700 m water depths (figure 2). The remaining elevated features have retained their conical shapes as they were originally emplaced at deeper depths and escaped the subaerial erosional activity. These observations allow us to suggest that the seamount highs A and B were emplaced above or close to the sea surface nearly 10 Myr after the emplacement of main plateau at 80–73 Ma.

Integrating all the new geophysical and geochronological data with existing magnetic data allowed the following emplacement phases of the ANS to be determined. Firstly, the undisturbed sequence of seafloor spreading anomalies 32n.1 through 34 (figure 3 and discussed in Krishna and Gopala Rao 2000; Krishna 2003), strongly suggests that the main plateau age is approximately the same age as the ocean floor beneath the seamount (80–73 Ma). This is in agreement with estimates of low elastic plate thickness (T_e) of 2–5 km for the seamount (Karner and Weissel 1990; Paul *et al.* 1990). All data are consistent with the ANS main plateau being constructed at a mid-ocean ridge simultaneously with the generation of new oceanic crust (figure 10a) and remained as a ridge crest feature (closely associated with Marion Dufresne, Lena and Ob seamounts emplaced on the Antarctic plate, see discussion below). Subsequently, late-stage volcanism (probably left-over melt within the main plateau) continued after c. 6–13 Myr (figure 10b) as shown by the $^{40}Ar/^{39}Ar$ ages of the basalt samples dredged from the shallowest parts of the seamount. This second-stage volcanism was volumetrically small (<1 % volume of the main plateau), probably limited to the elevated areas in the north, which is evident in the seamount morphology (see figure 2). It is generally observed that hotspots build a main edifice initially in a rather short magmatic period, and then can become active at a later time with a reduced volcanic activity. Examples of this phenomenon globally include the Hawaii, Canary, Reunion, Mauritius and Kerguelen islands. The best examples of late-stage or rejuvenated magmatic history are reported around the islands of O'ahu and Kaua'i along the Hawaiian chain (Garcia *et al.* 2010) and in Galapagos archipelago situated in Nazka plate (Geist *et al.* 2008). In Kaua'i Island region a 1 Myr gap was found prior to the onset of rejuvenated stage volcanism. The activity lasted for more than 2.45 Myr with a volume of about 0.1% of the total island edifice volume. Geist *et al.* (2008) hypothesised that the Galapagos hotspot with its episodic eruption of large lava flows between 3 and 2 Ma formed the archipelagic apron, upon which the island volcanoes were built at 3 Ma and again at 0.5 Ma. In the case of ANS, secondary elevated seamount highs (including seamount highs A and B) were formed c. 6–13 Myr later than the formation of the main plateau. It is not possible from existing data to constrain the length of the period of late-stage volcanism at ANS.

Geochemical analysis of samples from the ANS are consistent with previous observations (Mahoney *et al.* 1996; Borisova *et al.* 2001), and have depleted Nb, Ta, Th and U, and very low $^{206}Pb/^{204}Pb_{initial}$ of 17.23 and high $^{87}Sr/^{86}Sr_{initial}$ of 0.70672. The origin of very unusual geochemical signatures has been discussed by Mahoney *et al.* (1996) and Borisova *et al.* (2001), including contamination by ancient continental crust or mantle lithosphere, and is beyond the scope

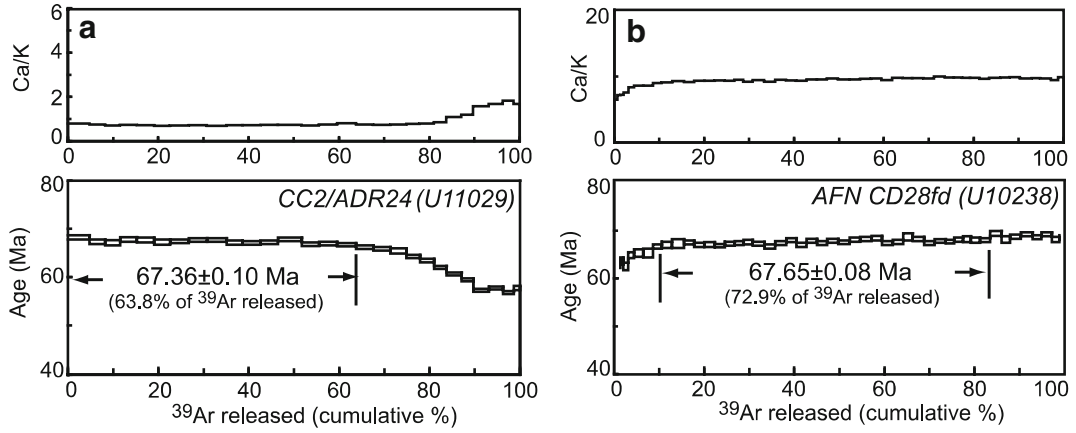

Figure 9. $^{40}Ar/^{39}Ar$ age spectra with Ca/K plot for ground-mass (CC2/ADR24) and feldspar (AFNCD28fd) samples of basalts from the Afanasy Nikitin seamount: (**a**) sample CC2/ADR24; (**b**) sample AFNCD28fd. Sample locations are shown in figure 2.

of this paper. However, the isotopic signatures of the ANS are not compatible with the Crozet or Marion hotspot sources, which exhibit distinctly higher $^{206}Pb/^{204}Pb_{initial}$ (18.17–19.23) and lower $^{87}Sr/^{86}Sr_{initial}$ (0.7039–0.7041) (Mahoney *et al.* 1996; Borisova *et al.* 1996).

We conjectured that the Conrad Rise hotspot was responsible for the formation of the Marion Dufresne, Lena and Ob seamounts (Diament and Goslin 1986; O'Neill *et al.* 2003) and the main plateau of the ANS during the period 80–73 Ma in a near spreading-ridge setting (figure 10a). The hotspot apparently had moved in its initial phase either side of the divergent plate boundary (India–Antarctica spreading ridge system), forming first the Marion Dufresne seamount on the Antarctic plate, followed by the main plateau of the ANS on Indian plate, before forming the Lena and Ob seamounts again on Antarctic plate and then remaining under the Antarctic plate until present.

6.2 *Different sources for the formation of the ANS and 85°E Ridge*

There are a number of lines of evidences to suggest that the ANS and 85°E Ridge arose from different mantle sources. Flexural analysis (Karner and Weissel 1990) and admittance analysis of the gravity data (Paul *et al.* 1990) for the ANS provide elastic plate thickness (T_e) values of 5 and 2–5 km, respectively. These low T_e values together with 18 km thick crustal model (Krishna 2003) indicate that the seamount initial load was emplaced at a mid-ocean ridge (India–Antarctica Ridge) concurrently with the generation of new oceanic crust. Interpretation of an unbroken sequence of linear magnetic anomalies 34–32n.2 (figure 3) over the main plateau of the ANS of late Cretaceous age (also see figure 1, Krishna and Gopala Rao 2000) also suggests an initial phase of volcanism in an on-ridge setting. On the other hand, isostatic and gravity modelling studies of profiles across the 85°E Ridge between 1°S and 15°N latitudes consistently show an elastic plate thickness of 10–15 km and flexural compensation beneath the ridge (Krishna 2003; Sreejith *et al.* 2011). These results suggest that the 85°E Ridge was emplaced substantially later (25–35 Myr) than the underlying oceanic lithosphere in an off-ridge setting, in contrast to the ANS. We do not observe any evidence for ridge jumps and/or relative motion of the mantle source contributing to variable T_e values and isostatic compensation. In recent studies of the 90°E Ridge, Krishna *et al.* (2012) have explained the tectonics associated with the emplacement of the ridge without the need for movement of the Kerguelen hotspot. Therefore, the contrasting elastic thicknesses and isostatic behaviours of the ANS and 85°E Ridge is supportive of differing mantle sources. For the ANS, one mantle-source generated the main plateau adjacent to the mid-ocean ridge, while for the 85°E Ridge another mantle source generated the aseismic ridge in an intra-plate setting.

Another line of evidence for different mantle sources comes from age and plate motion considerations. Between 6° and 18°N latitudes the 85°E Ridge is nearly linear in a north–south direction consistent with Indian plate northward motion from 90–42 Ma. Prior to 90 Ma the Indian plate moved in a northwest direction (Liu *et al.* 1983; Powell *et al.* 1988; Krishna *et al.* 2009a). With the consideration of Palaeocene activity of the ANS (Sborshchikov *et al.* 1995), 2600 km length of the 85°E Ridge track and emplacement rates of the

Table 1. *Results of stepwise-heating analyses of leached groundmass and feldspar of volcanic rocks from Afanasy–Nikitin seamount.*

Analysis no.	Sample no.	Material	Total gas age ($\pm1\sigma$)(Ma)	Seamount high age ($\pm1\sigma$)				Latitude (S)	Longitude (E)	Avg. water depth (m)
				Weighted average (Ma)	Inverse isochron age (Ma)	$^{40}Ar/^{36}Ar$ intercept	MSWD	Fraction of ^{39}Ar (%)			
U11029	CC2/ADR24	Groundmass	65.40 ± 0.05	67.36 ± 0.10	65.6 ± 0.7	2738 ± 2361	1.68	63.8	2°58.568'	82°51.015'	3350
U10238	AFNCD28fd	Plagioclase	67.57 ± 0.04	67.65 ± 0.08	67.5 ± 0.4	308 ± 17	1.67	72.9	3°6.5'	83°05'	2250

MSWD: Mean square of weighted deviates $(SUMS/(n-2)^{0.5})$ in York (1969).
Total gas ages were calculated using sum of the total gas released.
$\lambda_b = 4.962 \times 10^{-10}\ y^{-1}$, $\lambda_e = 0.581 \times 10^{-10}\ y^{-1}$, $^{40}K/K = 0.01167\%$ (Steiger and Jäger 1977).

90°E Ridge from late Cretaceous to early Cenozoic period, Krishna (2003) advocated that the 85°E Ridge track initiated in Mahanadi Basin at around 85 Ma and ended in the vicinity of north part of the ANS at about 55 Ma. In light of new results discussed in the present work, the above model suggested for the formation of the ANS needs to be reconsidered. If the ANS and 85°E Ridge were linked, then the new age of 67 Ma for the late-stage volcanism of the ANS implies an age for the northern part of the 85°E Ridge of ∼100 Ma (based on the length of the 85°E Ridge track and emplacement rate of the 90°E Ridge). In the case of consideration of shallow origin of the source for the 85°E Ridge, the emplacement rate for the ridge track significantly reduces following the relative plate motion. In such a situation, emplacement of 2600 km long 85°E Ridge track may even take longer than the assumed 30 Myr period (from ∼100 to 67 Ma), and may have started its initial activity very close to the age of break-up of the Eastern Continental Margin of India from east Antarctica. Therefore we argue that, irrespective of the depth of the source of material, that the 85°E Ridge track would have followed the NW motion of the Indian plate that prevailed before 90 Ma, and produced a change in the orientation of the initial part of the ridge track, which is not observed. In addition, a ridge with these estimated ages would have also provided a plate with an elastic plate thickness (T_e) of less than 10 km. Contrary to this, a linear N–S ridge track and 10–15 km thick T_e values are observed. In summary, this line of argument also suggests that the ANS and 85°E Ridge are not linked.

The morphology of the 85°E Ridge becomes less distinct south of 6°N, where the ridge track bends in a NNE–SSW direction between 6° and 2°N latitudes, before becoming N–S again between 2°N and 1°S latitudes. However, reasons for the bend in the southern component of the 85°E Ridge between 6° and 2°N remain unclear. We suggest that the hotspot that sourced the 85°E Ridge became weaker and ceased activity north of the ANS (figure 10c). There is no evidence for continuation of the hotspot to the position of the already extant ANS. Therefore, we believe that the 85°E Ridge was formed by a mantle source independent from the source that contributed to the formation of the ANS. Then the question arises – what source that caused the late-stage volcanism (67 Ma) over the existing main plateau of the ANS? Considering the geochemical and petrological signatures of the main plateau and seamount highs of the ANS from both published (Sborshchikov *et al.* 1995; Mahoney *et al.* 1996) and present studies, we envisage that the seamount highs may have been formed when the leftover melt that remained

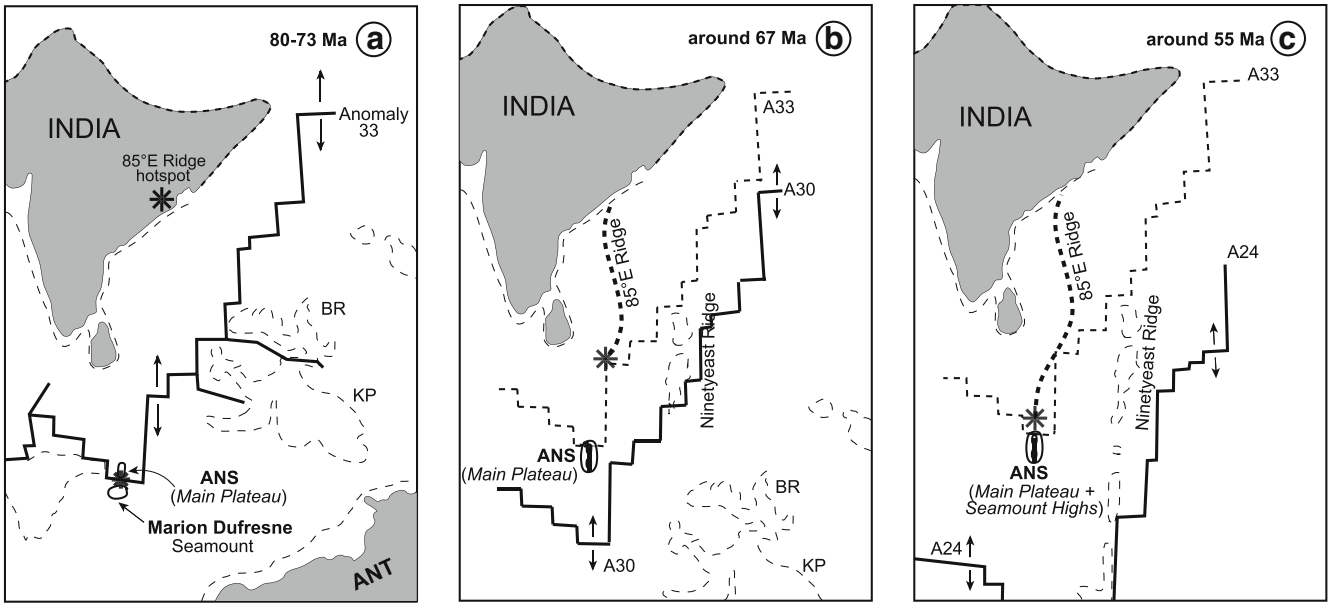

Figure 10. Sketch diagram showing the development of the ANS through time. Asterisk indicates the location of the hotspot that contributed to the formation of the 85°E Ridge from 85 to 55 Ma. (**a**) Emplacement of the main plateau of the ANS and Marion Dufresne seamount near the India–Antarctica Ridge between 80 and 73 Ma. (**b**) Renewed volcanism of the ANS at 67 Ma, and approximate position of the southern limit of the 85°E Ridge. Note the separation of the ANS and the southern end of 85°E Ridge at this time. (**c**) In subsequent times approximately at 55 Ma, the trace of the 85°E Ridge has come closer to the ANS and ceased. BR: Broken Ridge; KP: Kerguelen Plateau.

within the ANS plateau was released at 67 Ma in a flank- or off-ridge setting.

The present study, thus, explicitly brings out 67 Ma as the new age constraint for the secondary (late-stage) volcanism over the north part of main plateau of the ANS, but some element of ambiguity prevails with regard to the source – whether it was by the ANS or 85°E Ridge mantle source. Therefore, until we obtain additional constraints, other possible tectonic models for the formation of ANS and 85°E Ridge proposed by Curray and Munasinghe 1991; Müller *et al.* 1993 and Krishna (2003) cannot be overlooked. New scientific experiments involving Ocean Bottom Seismometric (OBS) observations over the 85°E Ridge and possible collection of ridge rock samples, may add additional constraints of velocity structure and dates. These eventually may single out the geological processes of formation of both the ANS and 85°E Ridge.

7. Summary and conclusions

Study of new multibeam bathymetric and seismic reflection and previous magnetic data over the Afanasy Nikitin seamount, together with newly determined dates of the dredged samples, has provided valuable insights into the growth of the ANS through time, and its relationship with the 85°E Ridge.

- Seafloor morphology and seismic structure of the ANS show that the seamount encompasses an extensive plateau (called the main plateau) with an elevation of about 1200 m above the adjacent ocean floor (4800 m water depth). In the northern part of the seamount numerous elevated features (called seamount highs) pierce through the main plateau, whereas in the southern part, N–S oriented fault planes have broken the plateau into structural blocks. Geomorphology and subsidence process are supportive of two phases of seamount construction. Two shallow edifices (at 1600 and 2050 m) have the morphology of a guyot, suggesting that they were formed close to sea-level during the phase of late-stage volcanism and topping the 'main plateau'.
- Seafloor spreading anomalies 34 through 32n.1, low (2 – 5 km) T_e values (Karner and Weissel 1990; Paul *et al.* 1990) and ∼18 km thick crust beneath the ANS (Krishna 2003) suggest that the main plateau of the ANS was formed in an initial phase of volcanism in an on-ridge setting at 80–73 Ma. Based on present results and published plate reconstruction results of the Indian Ocean, we believe that the Conrad Rise hotspot has emplaced both the main plateau of the ANS and Conrad Rise (including the Marion Dufresne seamount) together during the period 80–73 Ma, close to the India–Antarctica spreading ridge system. Thereafter the hotspot has shifted its activity to Antarctic plate leaving the main

plateau of the ANS as an isolated feature on the Indian plate. Ages determined by $^{40}Ar/^{39}Ar$ dating for two basalt samples from the Afanasy Nikitin seamount highs of 67.36 ± 0.10 Ma and 67.65 ± 0.08 Ma are indistinguishable within 2σ. The 67 Ma date suggests that late-stage volcanism occurred with reduced activity c. 6–13 Myr after the constructional phase of the main plateau of the ANS.

- Elastic plate thickness (T_e) values and isostatic behaviour of the 85°E Ridge and ANS are at variance. They, together with plate motion data, suggest that the structures may have been formed by different mantle sources. No evidence is found for continuation of the hotspot that formed the 85°E Ridge to the position of the already extant ANS. Therefore, it is interpreted that the 85°E Ridge was formed by a mantle source independent from the source that contributed to the formation of the ANS. Late-stage volcanism (67 Ma) over the existing main plateau of the ANS may have occurred when the leftover melt, remaining within the ANS plateau was released in a flank- or off-ridge setting.

Acknowledgements

KSK thanks the Royal Society for their award of a RS–CSIR Fellowship to support this research at the National Oceanography Centre, Southampton and at the University of Edinburgh. OI greatly appreciates JSPS for supporting a Japan–UK joint research program. The authors thank M Narui and M Yamazaki, International Research Center for Nuclear Materials Science, Institute for Materials Research, Tohoku University for providing opportunities of neutron irradiation of samples at the JRR3 reactor. They also thank K Yamanobe for assistance with geochemical analyses and are grateful to the Ministry of Earth Sciences, India for the support extended for the acquisition of multibeam bathymetry and other oceanographic data over the ANS. This is NIO contribution number 5416.

Appendix

Laser step-heating experiments were conducted on 22 mg of plagioclase separates in case of sample AFNCD28fd and 11.4 mg of ground-mass separate for sample CC2/ADR24. Due to weak alteration in poorly-crystallized part of ground-mass, samples were treated at 100°C on hot plate with stirrer in 6N HCl for 60 min and then 6N HNO_3 for 60 min in order to eliminate possible alteration products (clays and carbonates) prior to irradiation. After this acid treatment, these separates were examined under binocular microscope before being packed for irradiation. Sample irradiation was done at the JRR3 reactor of Japan Atomic Energy Agency. Fast neutron fluxes were about 1.4–1.7 $\times$ 10^{12} n/cm^2·s. Sanidine separated from the Fish Canyon Tuff (FC3) was used for the flux monitor and assigned an age of 27.5 Ma, which has been determined against our primary standard for our K–Ar laboratory, Sori biotite, whose age is 91.2 Ma (Uchiumi and Shibata 1980).

CO_2 laser (NEWWAVE MIR10-30) equipped with a faceted lens was used for sample heating. Argon isotopes were measured on a VG Isotech VG3600 noble gas mass spectrometer fitted with a BALZERS electron multiplier. Correction for interfering isotopes was achieved by analyses of $CaFeSi_2O_6$ and $KFeSiO_4$ glasses irradiated with the samples. The blank of the system including the mass spectrometer and the extraction line was 7.5 $\times$ 10^{-14} ml STP for ^{36}Ar, 2.5 $\times$ 10^{-13} ml STP for ^{37}Ar, 2.5 $\times$ 10^{-13} ml STP for ^{38}Ar, 1.0 $\times$ 10^{-12} ml STP for ^{39}Ar and 2.5 $\times$ 10^{-12} ml STP for ^{40}Ar. The blank analysis was done every 2 or 3 step analyses.

Errors for ages include analytical uncertainties for Ar isotope analysis, correction for interfering isotopes and J value estimation. An error of 0.5% was assigned to J values as a pooled estimate during the course of this study. Plateau ages were calculated as weighted means of ages of plateau-forming steps, where each age was weighted by the inverse of its variance. The age plateaus were determined following the definition by Fleck *et al.* (1977). Inverse isochrons were calculated using York's least-squares fit, which accommodates errors in both ratios and correlations of errors (York 1969).

References

Banakar V K, Pattan J N and Mudholkar A V 1997 Paleoceanographic conditions during the formation of a ferromanganese crust from the Afanasy–Nikitin seamount, north central Indian Ocean: Geochemical evidence; *Mar. Geol.* **136** 299–315.

Bull J M 1990 Structural style of intraplate deformation, central Indian Ocean Basin: Evidence for the role of fracture zones; *Tectonophys.* **184** 213–228.

Bull J M and Scrutton R A 1992 Seismic reflection images of intraplate deformation, central Indian Ocean, and their tectonic significance; *J. Geol. Soc. London* **149** 955–966.

Borisova A Yu, Nikulin V V, Belyatsky B V, Ovchinnikova G V, Lewskii L K and Sushvhevskaya N M 1996 Late alkaline lavas of the Ob and Lena Seamounts (Conrad Rise, Indian Ocean): Geochemistry and characterisation of mantle sources; *Geochem. Int.* **34** 503–517 (in Russian).

Borisova A Yu, Belyatsky B V, Portnyagin M V and Sushchevskaya N M 2001 Petrogenesis of Olivine-phyric Basalts from the Aphanasey Niktitin Rise: Evidence for contamination by Cratonic Lower Continental Crust; *J. Petrol.* **42** 277–319.

Cande S C and Kent D V 1995 Revised calibration of the geomagnetic polarity time scale for the Late Cretaceous and Cenozoic; *J. Geophys. Res.* **100** 6093–6095, doi: 10.1029/94JB03098.

Curray J R and Munasinghe T 1991 Origin of the Rajmahal Traps and the 85°E Ridge: Preliminary reconstructions of the trace of the Crozet hotspot; *Geology* **19** 1237–1240.

Curray J R, Emmel F J, Moore D G and Russel W R 1982 Structure, tectonics, and geological history of the northeastern Indian Ocean; In: *The Ocean Basins and Margins, The Indian Ocean* (eds) Nairn A E and Stehli F G, Plenum, New York, **6** 399–450.

Diament M and Goslin J 1986 Emplacement of the Marion Dufresne, Lena and Ob seamounts (South Indian Ocean) from a study of isostasy; *Tectonophys.* **121** 253–262.

Fleck R J, Sutter J F and Elliot D H 1977 Interpretation of discordant $^{40}Ar/^{39}Ar$ age-spectra of Mesozoic tholeiites from Antarctica; *Geochim. Cosmochim. Acta* **41** 15–32.

Garcia M O, Swinnard L, Weis D, Greene A, Tagami T, Sano H and Gandy C 2010 Petrology, geochemistry and geochronology of Kaua'i Lavas over 4.5 Myr: Implications for the origin of rejuvenated volcanism and the evolution of the Hawaiian plume; *J. Petrol.* **51** 1507–1540.

Geist D, Diefenbach B A, Fornari D J, Kurz M D, Harpp K and Blusztajn J 2008 Construction of the Gala'pagos platform by large submarine volcanic terraces; *Geochem. Geophys. Geosys.* **9** Q03015, doi: 10.1029/2007GC001795.

Gopala Rao D, Krishna K S and Sar D 1997 Crustal evolution and sedimentation history of the Bay of Bengal since the Cretaceous; *J. Geophys. Res.* **102** 17,747–17,768.

Ishizuka O, Yuasa M, Taylor R N and Sakamoto I 2009 Two contrasting magmatic types coexist after the cessation of back-arc spreading; *Chem. Geol.* **266** 283–305.

Karner G D and Weissel J K 1990 Compressional deformation of oceanic lithosphere in the central indian Ocean: Why it is, where it is; In: *Proc. Ocean Drilling Program* (eds) Cochran J R, Stow D A V *et al.*, *Sci. Results*, College Station, Texas, Ocean Drilling Program, **116** 279–289.

Krishna K S, Gopala Rao D, Ramana M V, Subrahmanyam V, Sarma K V L N S, Pilipenko A I, Shcherbakov V S and Radhakrishna Murthy I V 1995 Tectonic model for the evolution of oceanic crust in the northeastern Indian Ocean from the Late Cretaceous to the Early Tertiary; *J. Geophys. Res.* **100** 20,011–20,024.

Krishna K S, Ramana M V, Gopala Rao D, Murthy K S R, Rao M M M, Subrahmanyam V and Sarma K V L N S 1998 Periodic deformation of oceanic crust in the central Indian Ocean; *J. Geophys. Res.* **103** 17,859–17,875.

Krishna K S and Gopala Rao D 2000 Abandoned Paleocene spreading center in the northeastern Indian Ocean: Evidence from magnetic and seismic reflection data; *Mar. Geol.* **162** 215–224.

Krishna K S, Bull J M and Scrutton R A 2001 Evidence for multiphase folding of the central Indian Ocean lithosphere; *Geology* **29** 715–718.

Krishna K S 2003 Structure and evolution of the Afanasy Nikitin seamount, buried hills and 85°E Ridge in the northern Indian Ocean; *Earth Planet. Sci. Lett.* **209** 379–394.

Krishna K S, Michael L, Bhattacharyya R and Majumdar T J 2009a Geoid and gravity anomaly data of conjugate regions of Bay of Bengal and Enderby Basin – new constraints on breakup and early spreading history between India and Antarctica; *J. Geophys. Res.* **114** B03102, doi: 10.1029/2008JB005808.

Krishna K S, Bull J M and Scrutton R A 2009b Early (pre-8 Ma) fault activity and temporal strain distribution in the central Indian Ocean; *Geology* **37** 227–230.

Krishna K S, Abraham H, Sager W W, Pringle M, Frey F A, Gopala Rao D and Levchenko O V 2012 Tectonics of the Ninetyeast Ridge derived from the spreading records of the contiguous oceanic basins and age constraints of the ridge; *J. Geophys. Res.* **117**, doi: 10.1029/2011JB008805.

Liu C S, Curray J R and McDonald J M 1983 New constraints on the tectonic evolution of the Eastern Indian Ocean; *Earth Planet. Sci. Lett.* **65** 331–342.

Mahoney J J, White W M, Upton B G J, Neal C R and Scrutton R A 1996 Beyond EM-1: Lavas from Afanasy–Nikitin Rise and the Crozet Archipelago, Indian Ocean; *Geology* **24** 615–618.

Michael L and Krishna K S 2011 Dating of the 85°E Ridge (northeastern Indian Ocean) using marine magnetic anomalies; *Curr. Sci.* **100** 1314–1322.

Müller R D, Royer J-Y and Lawver L A 1993 Revised plate motions relative to the hotspots from combined Atlantic and Indian Ocean hotspot tracks; *Geology* **21** 275–278.

O'Neill C, Müller R D and Steinberger B 2003 Geodynamic implications of moving Indian Ocean hotspots; *Earth Planet. Sci. Lett.* **215** 151–168.

Paul J, Singh R N, Subrahmanyam C and Drolia R K 1990 Emplacement of Afanasy–Nikitin seamount based on transfer function analysis of gravity and bathymetry data; *Earth Planet. Sci. Lett.* **96** 419–426.

Powell C M, Roots S R and Veevers J J 1988 Pre-breakup continental extension in east Gondwanaland and the early opening of the eastern Indian Ocean; *Tectonophys.* **155** 261–283.

Radhakrishna M, Srinivasa Rao G, Nayak S, Bastia R and Twinkle D 2012 Early Cretaceous fracture zones in the Bay of Bengal and their tectonic implications: Constraints from multi-channel seismic reflection and potential field data; *Tectonophys.* **522–523** 187–197.

Redbourn L J, Bull J M, Scrutton R A and Stow D A V 1993 Channels, echo character mapping and tectonics from 3.5 kHz profiles, distal Bengal Fan; *Mar. Geol.* **114** 155–170.

Royer J-Y and Sandwell D T 1989 Evolution of the eastern Indian Ocean since the Late Cretaceous: Constraints from Geosat Altimetry; *J. Geophys. Res.* **94** 13,755–13,782.

Royer J-Y, Peirce J W and Weissel J K 1991 Tectonic constraints on the hot-spot formation of Ninetyeast Ridge; In: *Proc. ODP, Sci. Results*, College Station, Texas, Ocean Drilling Program, **121** 763-776.

Sborshchikov I M, Murdmaa I O, Matveenkov V V, Kashintsev G L, Glomshtock A I and Al'mukhamedov A I 1995 Afanasy Nikitin seamount within the intraplate deformation zone, Indian Ocean; *Mar. Geol.* **128** 115–126.

Sreejith K M, Radhakrishna M, Krishna K S and Majumdar T J 2011 Development of the negative gravity anomaly of the 85°E Ridge, northeastern Indian Ocean – a process oriented modeling approach; *J. Earth Syst. Sci.* **120** 605–615.

Steiger R H and Jäger E 1977 Subcommision on geochronology: Convention on the use of decay constants in geo- and cosmochronology; *Earth Planet. Sci. Lett.* **36** 359–362.

Uchiumi S and Shibata K 1980 Errors in K–Ar age determination; *Bull. Geol. Surv. Japan* **31** 267–273 (in Japanese with English abstract).

York D 1969 Least squares fitting of a straight line with correlated errors; *Earth Planet. Sci. Lett.* **5** 320–324.

MS received 15 January 2013; revised 2 July 2013; accepted 5 July 2013